DOCUMENT CONTROL SHEET

	ORIGINATOR'S REF.		SECURITY CLASS.
	NLR TP 96487 U		Unclassified

ORIGINATOR
National Aerospace Laboratory NLR, Amsterdam, The Netherlands

TITLE
Fully automatic Navier-Stokes Algorithm for 2D high-lift flows

PRESENTED AT
the 15th International Conference on Numerical Methods in Fluid Dynamics, June 24-28, 1996, Monterey, California, USA. The paper is related to work carried out under a contract awarded by the Netherlands Agency for Aerospace Programs, contract number 01308N

AUTHORS	DATE	pp	ref
K.M.J. de Cock	960807	10	15

DESCRIPTORS

Airfol profiles	Turbulence models
Algorithms	Two dimensional flow
Lift devices	Unstructured grids (mathematics)
Multigrid methods	Viscous flow
Navier-Stokes equation	Wing flaps
Separated flow	

ABSTRACT
A description of a Fully Automatic Navier-Stokes algorithm for 2D High-Lift flows is given. The effectiveness of multi grid to solve the steady, compressible Reynolds Averaged Navier-Stokes and $\kappa - \omega$ turbulence equations on 2D unstructured grids to second order accuracy is demonstrated. Results are shown for both transonic and High-Lift cases.

NLR TECHNICAL PUBLICATION

TP 96487 U

FULLY AUTOMATIC NAVIER-STOKES ALGORITHM FOR 2D HIGH-LIFT FLOWS

by

K.M.J. de Cock

This paper was presented at the 15th International Conference on Numerical Methods in Fluid Dynamics, June 24-28, 1996, Monterey, California, USA. The paper is related to work carried out under a contract awarded by the Netherlands Agency for Aerospace Programs, contract number 01308N.

Division : Fluid Dynamics
Prepared : KMJdC/ C
Approved : BO/ BO

Completed : 960807
Order number : 526.101
Typ. : LMT

Contents

11 Figures

(10 pages in total)

List of symbols

k	turbulent kinetic energy,
ϵ	dissipation of k,
ω	specific dissipation rate of k,
ω_b	back ground specific dissipation rate of k,
ρ	density,
D_k	dissipation term of the k equation,
D_ω	dissipation term of the ω equation,
β^*	model coefficient corresponding to D_k,
β	model coefficient corresponding to D_ω,
M	Mach number,
α	angle of attack,
c	chord,
Re_c	Reynolds number based on the chord c,
c_l	lift coefficient,
c_d	drag coefficient,
c_m	moment coefficient,
c_p	pressure coefficient,
Tu	degree of turbulence,
q_∞	free stream velocity,
Δp_t	total pressure loss,

Fully Automatic Navier-Stokes algorithm for 2D High-Lift flows [1]

K.M.J. de Cock
NLR, Anthony Fokkerweg 2, 1059 CM Amsterdam,
The Netherlands, +31-(0)20-511 34 49, cock@nlr.nl

Abstract

A description of a Fully Automatic Navier-Stokes algorithm for 2D High-Lift flows is given. The effectiveness of multi grid to solve the steady, compressible Reynolds Averaged Navier-Stokes and k - ω turbulence equations on 2D unstructured grids to second order accuracy is demonstrated. Results are shown for both transonic and High-Lift cases.

Introduction

Design of High-Lift devices to achieve specific maximum lift values is of great importance for the wing sizing of large aircraft. Aerodynamic analysis codes based on Viscous-Inviscid Interaction methods are still frequently used due to desirable properties with respect to turn around times and computational cost. Limitations on the physical modeling triggered the use of (multi block structured) Reynolds Averaged Navier-Stokes (RANS) methods, capable of computing accurate solutions. A new bottleneck however is the generation of multi block grids, causing large turn around times. Pioneering work to overcome this grid generation problem with unstructured grids has been conducted by D. Mavriplis, Ref. 6, using a k-ϵ turbulence model.

This paper covers a 2D Fully Automatic Navier-Stokes (FANS) algorithm for High-Lift flows on unstructured grids. The algorithm is based on the compressible RANS equations coupled to the standard two equation k - ω turbulence model.
The main objectives of this paper are : 1) demonstrate the effectiveness of the multi grid (MG) for a second order accurate discretization of the RANS and the k - ω turbulence equations on unstructured grids, 2) illustrate that a two equation turbulence model is the lowest level of turbulence modeling capable of predicting wake boundary layer confluence without ad hoc fixes to determine the turbulent length scale.

2D unstructured grid generation for viscous flow simulations

The following steps in the automatic grid generation process can be distinguished :

Step 1, regularization of the geometric singularities on a small scale (typically 0.01 % chord), in order to make step 2 and 4 robust, Fig. 1b. In combination with step 3, step 1 causes an automatic reduction of the aspect ratio of the grid near trailing edges by clustering grid points. In 3D this clustering is also desirable for accuracy and robustness of the flow solver, but not yet acceptable.

[1] This investigation was performed under contract 01308N with the Netherlands Agency for Aerospace Programs (NIVR).

Step 2, creation of a Wall Proximity Region (WPR) by inflating the geometry, resulting in two different domains in which different flow phenomena occur. This WPR should cover the high velocity gradient region of a turbulent wall bounded flow (only a part of the total thickness). Fig. 1a shows the original and inflated geometry for the NACA 0012 airfoil, and Fig. 1b shows a detail of the last 0.5 % chord (regularization of a sharp trailing edge, step 1).

Step 3, creation of an Euler grid suited for MG outside the WPR, with automatic refinement towards the geometry and in regions of high geometric curvature. For thin WPR the properties of the original geometry are sufficiently reflected in the inflated geometry. Compared to Ref. 7, no background grid with user defined sources is used. For further details, see Ref. 12.

Step 4, algebraic generation of a structured, O-type Navier-Stokes grid in the WPR, made unstructured by uniformly created diagonals and agglomerated in normal direction. Advantages with respect to accuracy are : a smooth variation of the control volume shape, a constant, low stretching of the grid in normal direction, a better accuracy due to the central symmetry property (Ref. 13), and a constant number of connections per grid node. An other, practical advantage is that the algorithm uses only one element type. In 3D, it is no longer possible to create diagonals in a uniform way, hence a mixture of prisms and tetrahedra is to be preferred.

Flow solver

The steady, compressible RANS equations are solved, coupled to the standard k - ω two equation turbulence model, Ref. 3. A modification to the k - ω production term according to Ref. 1 is considered, in order to avoid unphysical production in stagnation, separation and reattachment zones. The following dissipation terms are used

$$D_k = \beta^* \rho k \left(\omega - \omega_b\right) sign(\omega - \omega_b), \qquad D_\omega = \beta \rho \left(\omega - \omega_b\right)^2 sign(\omega - \omega_b).$$

with the density ρ, the turbulent kinetic energy k, the specific dissipation rate ω, the background specific dissipation rate ω_b, the model coefficients β^* and β, and the sign function. For ω_b equal to zero, the classical dissipation terms are recovered. With these dissipation terms the asymptotic value of ω in regions with no production tends to a background value ω_b, without changing the basic behavior of k. Due to this modification, the frequently used limiter on ω to avoid singularities of the turbulent viscosity, $\omega_{limited} = max(\omega, \omega_b)$, can be omitted (if active, this limiter hampers MG convergence due to non vanishing residuals). A cross diffusion term according to Wilcox is implemented to reduce the dependency of the solution of the k-ω equations on the value of ω at the edge of the viscous layers, Ref. 2.

Adiabatic, no-slip boundary conditions are used for solid walls. The turbulent kinetic energy is zero at the wall and the boundary condition for ω is found from modeling the roughness of the wall.

Standard discretization techniques are used to discretize the governing equations (Ref 15, 12), including upwind flux difference discretization for the convective fluxes, central discretization for the viscous fluxes and point implicit discretization for the source terms. Assuming a constant representation of the solution within a finite volume, this results in

a first order accurate scheme which can be solved by Jacobi relaxation within a standard Full Approximation Scheme (FAS) MG. Linear interpolation is used for the prolongation and restriction operators, and injection is used for the projection operator. Remark that due to the constant representation of the solution adopted within a finite volume, the production and the cross diffusion in the volume are zero, since these terms are driven by gradients of the solution. This is desirable since these terms spoil the smoothing properties of the discretized equations. Second order accuracy of the complete set of equations on the highest grid level is obtained using a linear representation of the solution (Refs. 5, 11), and a defect correction MG technique. As a consequence, the contributions of the production and cross diffusion terms are included in the defect correction. Solving the turbulence equations also with second order accuracy is a novel aspect of the present approach. Common practise is to solve the turbulence equations only to first order spatial accuracy (Refs. 6, 9).

Results

Three cases are discussed :

Case 1, NACA 0012 profile, transonic flow with $M = 0.799$, $\alpha = 2.26$, $Re_c = 9\text{x}10^6$, free transition, 46084 nodes in the highest grid level, 32 nodes per boundary layer station. In Fig. 2 good agreement with Ref. 2 is demonstrated for the pressure coefficient c_p of this transonic case with shock induced separation. Ref. 2 also discusses a modification of the turbulence model necessary to find the experimentally observed shock location.

Case 2, NLR 7301 profile + flap, High-Lift flow with $M = 0.185$, $\alpha = 13.1$, $Re_c = 2.51\text{x}10^6$, flap gap 2.6%c, fixed transition at 3.3%c on the upper wing surface, 72.5%c on the lower wing surface, and 105.7%c on the flap upper surface, 44000 nodes in the highest grid level, 32 nodes per boundary layer station. The transition locations are obtained from experiments. Force coefficients : $c_l = 3.0475$ (experiment 2.3% lower), $c_d = 0.0570$ (experiment 28% lower, but obtained from wake traverse), $c_m = -0.4755$ (experiment 8% higher). This is consistent with structured grid CFD results in Ref. 4.

Case 3, NLR 422 three element airfoil, High-Lift flow with $M = 0.3$, $\alpha = 8$, $Re_c = 6\text{x}10^6$, free transition, 28955 nodes in the highest grid level, 16 nodes per boundary layer station.

MG performance is discussed first. The normalized maximum residuals of the mass, k and ω equation drop between 3.5 and 4.5 orders of magnitude in 500 MG V-cycles for both case 1 (Fig. 1) and case 2 (Fig. 2). Remark that it takes about 100 V-cycles to obtain velocity profiles that generate net production of k at the wall. Five MG levels are used for all cases. Level 4 is formed by global coarsening level 5, and level 1,2 and 3 are generated by semi coarsening level 4 normal to the wall in the WPR. Grid level 4 for case 2 is shown in Fig. 5. Semi coarsening of the grid is mainly used for robustness, suppose that global coarsening is used to generate grid level 1 to 4. In that case, the same grid resolution in normal direction at the wall will be found on grid level 1 as with semi coarsening. The grid in tangential direction however will be too coarse in order to generate useful MG corrections for difficult flow cases (for instance separation bubbles).

Secondly, High-Lift results are shown. In Figs. 6 and 7 the computed c_p of case 2 is

compared with the experimental values of Ref. 10. A laminar separation bubble is found just before the transition location on the upper wing surface. Although the c_p on the flap seems to be close to the experiment, a discrepancy exists on the flap upper surface, due to the turbulence model predicting an excessive shear in the wake of the wing. This causes an underprediction of the wake dispacement, see Ref. 14. For this discrepancy the k - ω modification discussed in Ref. 2 can partly bring relief.
Further, compared to for instance Ref. 7, 8, a turbulent length scale equation is used to define the length scales in the region above the flap. This is also necessary for the three element airfoil flow of case 3. In Fig. 8 grid level 4 is shown, and in Fig. 9 an isoline of the degree of turbulence $Tu = \sqrt{2/3k}/q_\infty = 4\%$, demonstrating the confluence of the turbulent wake of the slat with the boundary layer of the wing. In Fig. 10 Mach isolines are shown around the slat. A small supersonic region is present, requiring the use of the compressible RANS equations. In Fig. 11 total pressure loss Δp_t isolines are given in the flap region. Separation occurs at the flap trailing edge.

Conclusions

Good multi grid performance of the second order accurate discretized RANS and k-ω equations is demonstrated for a transonic and a High-Lift flow, both involving separated regions. High-Lift flow results are shown using a two equation turbulence model which is the lowest level of turbulence modeling capable of simulating the merging of a wake with a boundary layer without ad hoc fixes to the turbulence model. This level of turbulence modeling combined with the automatic grid generation and the good multi grid performance results in a very powerful tool to analyze the maximum lift capability of different High-Lift configurations.

References

1. F.R. Menter: AIAA-93-2906 (1993)
2. M. Kandula, D.C. Wilcox: AIAA-95-2317 (1995)
3. D.C. Wilcox: AIAA-93-2905 (1993)
4. W. Haase: Notes on Numerical Fluid Mechanics, Vol 42, Vieweg (1993)
5. V. Venkatakrishnan: JCP 118 (1995)
6. D.J. Mavriplis: ICASE 91-11 (1991)
7. G.A. Ashford, K.G. Powell: AIAA-95-1724-CP (1995)
8. D.L. Marcum, N.P. Weatherill, M.J. Marchant, F. Beaven: AIAA-95-1726-CP (1995)
9. E. Monsen, R. Rudnik: AIAA-95-0089 (1995)
10. B. van den Berg: NLR TR 79009 U (1979)
11. M. Aftosmis: AIAA 93-0772 (1993)
12. K. de Cock: NLR TP 93301 (1993)
13. J.W. van der Burg, J.E.J Maseland, B. Oskam: NLR TP 96036 (1996)
14. B. Oskam, D.J. Laan, D.F. Volkers: NLR MP 84042 (1984)
15. E. Dick, J. Steelant: AIAA 95-1669 (1995)

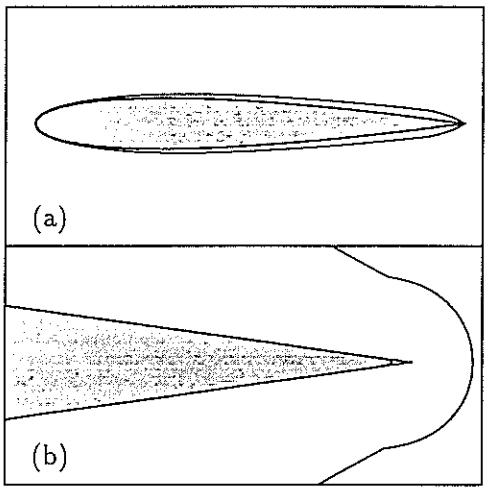

Fig. 1 NACA 0012, (a) geometry and WPR, (b) detail of the last 0.5%c

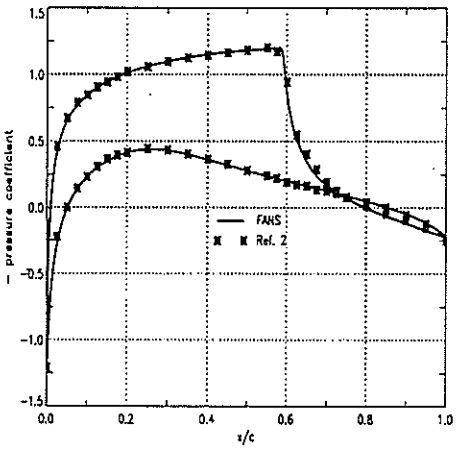

Fig. 2 NACA 0012, $M = .799$, $\alpha = 2.26$, $Re_c = 9\text{x}10^6$, cp distribution

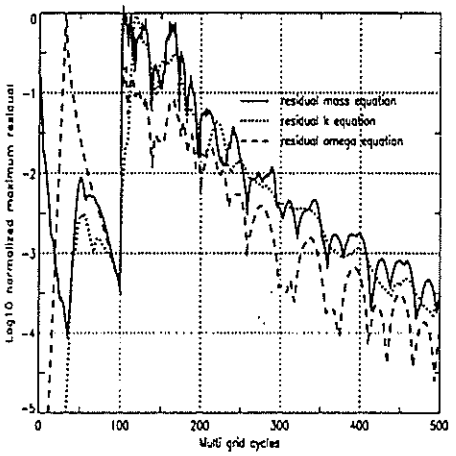

Fig. 3 NACA 0012, $M = .799$, $\alpha = 2.26$, $Re_c = 9\text{x}10^6$, convergence history

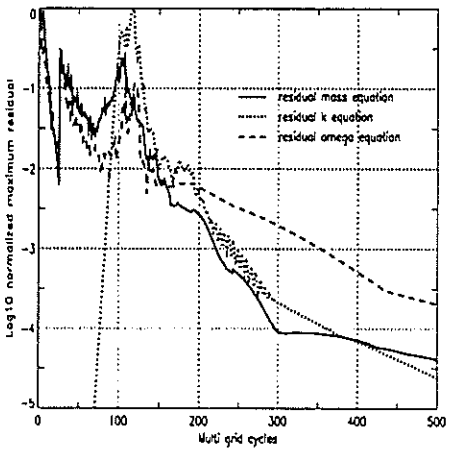

Fig. 4 NLR 7301 + flap, $M = .185$, $\alpha = 13.1$, $Re_c = 2.51\text{x}10^6$, convergence history

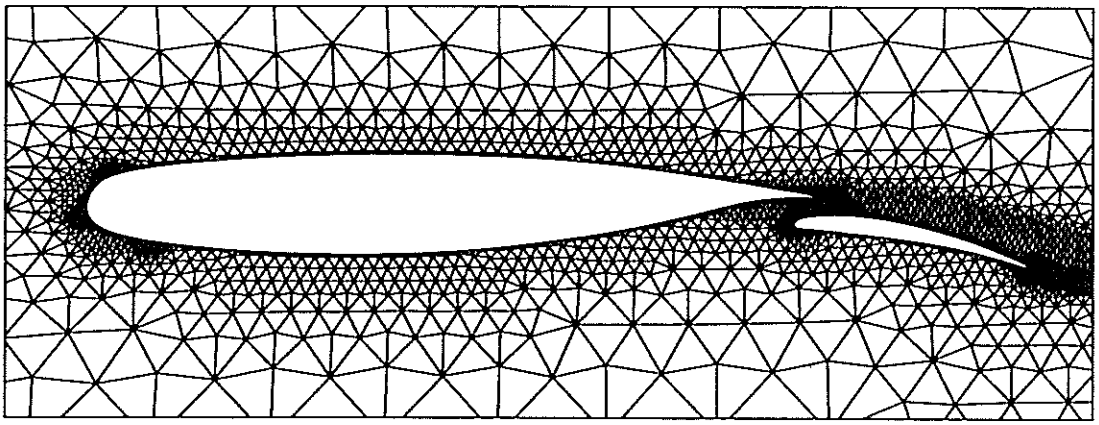

Fig. 5 NLR 7301 + flap, grid level number 4 out of 5

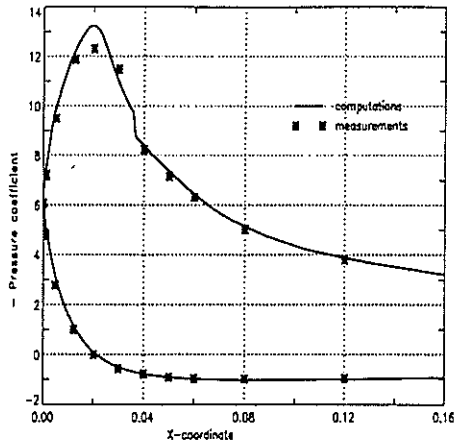

Fig. 6 NLR 7301 + flap, $M = .185$, $\alpha = 13.1$, $Re_c = 2.51\text{x}10^6$, c_p on the wing

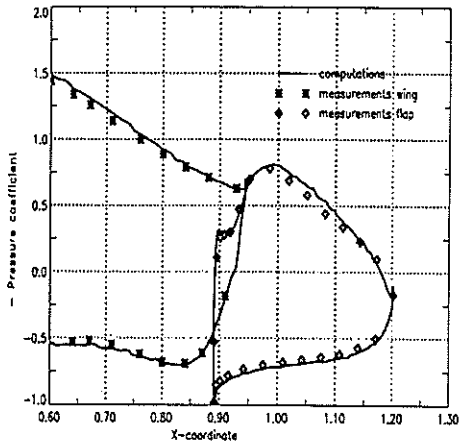

Fig. 7 NLR 7301 + flap, $M = .185$, $\alpha = 13.1$, $Re_c = 2.51\text{x}10^6$, c_p on the flap

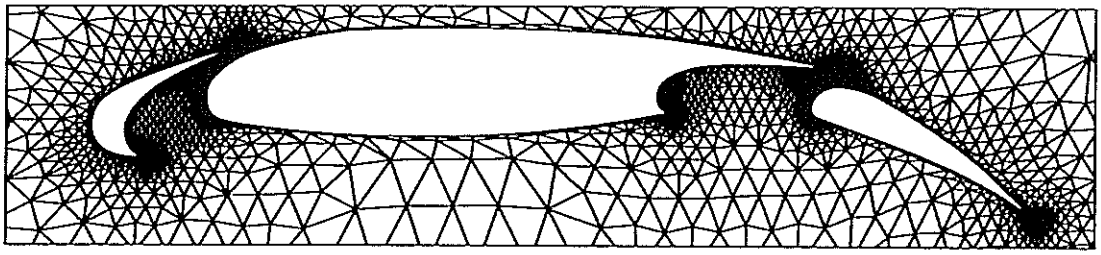

Fig. 8 NLR 422, grid level number 4 out of 5

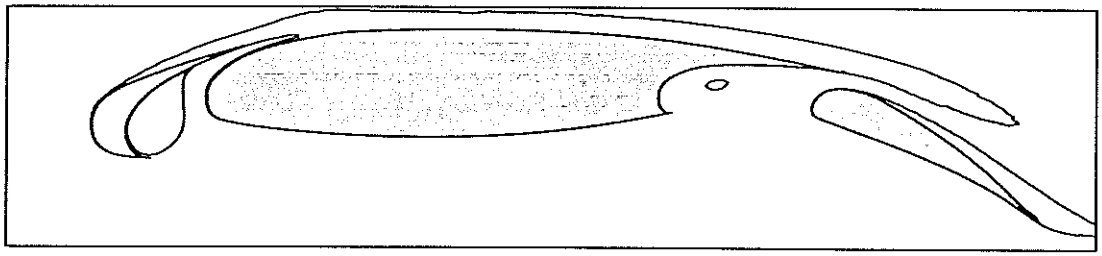

Fig. 9 NLR 422, $M = 0.3$, $\alpha = 8$, $Re_c = 6\text{x}10^6$, isoline of the turbulence degree $Tu = 4\%$

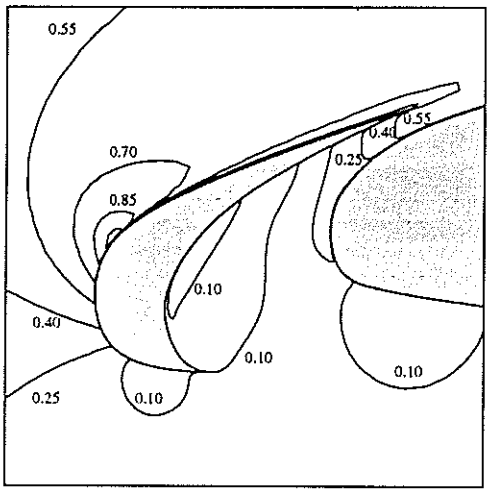

Fig. 10 NLR 422, $M = 0.3$, $\alpha = 8$, $Re_c = 6\text{x}10^6$, $M = 0.10, 0.25, 0.40, ..., 1.00$

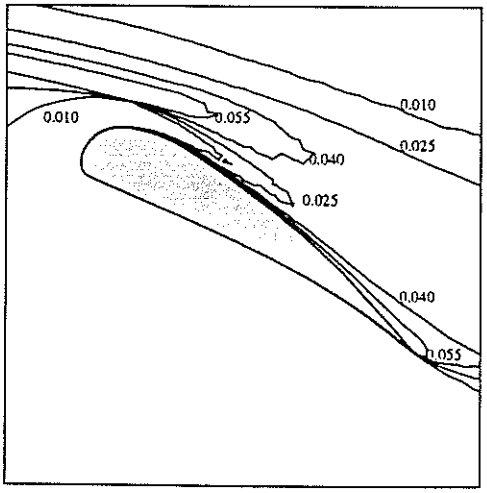

Fig. 11 NLR 422, $M = 0.3$, $\alpha = 8$, $Re_c = 6\text{x}10^6$, $\Delta p_t = 0.010, 0.025, 0.040, 0.055$